# Paper 2

**The Phase Field Theory Applied to $CO_2$ and $CH_4$ Hydrate**

*Atle Svandal, Bjørn Kvamme, László Gránásy, Tamás Pusztai, Trygve Buanes, Joakim Hove*

Journal of Crystal Growth, **287**, p485-490, (2006)

Available online at www.sciencedirect.com
SCIENCE DIRECT®
Journal of Crystal Growth 287 (2006) 486–490
JOURNAL OF CRYSTAL GROWTH
www.elsevier.com/locate/jcrysgro

# The phase-field theory applied to $CO_2$ and $CH_4$ hydrate

Atle Svandal[a,*], Bjørn Kvamme[a], Làszlò Gràànàsy[b], Tamàs Pusztai[b], Trygve Buanes[a], Joakim Hove[a]

[a]*Department of Physics and Technology, University of Bergen, Allègaten 55, N-5007 Bergen, Norway*
[b]*Research Institute for Solid State Physics and Optics, H-1525 Budapest, POB 49, Hungary*

Available online 4 January 2006

**Abstract**

A phase-field theory is applied to model the growth of carbon dioxide hydrate and methane hydrate from a supersaturated solution in water. Temperature- and pressure-dependent thermodynamics for the two systems are accounted for. Simulations of the growth of a planar hydrate film and a circular hydrate nucleus are presented and the interface velocity has been extrapolated from the results to experimental time scales. We discuss how pressure and temperature affects the growth rate and argue that the governing process for the dynamics is the chemical diffusion of the guest molecule in the aqueous solution. We also present results from anisotropic simulations and outline how this will affect the growth.


*PACS:* 2001:81.10.Aj; 81.10.Dn; 82.60Lf

*Keywords:* A1. Diffusion; A1. Gas hydrate; A1. Phase-field theory; B1. Carbon dioxide; B1. Methane

## 1. Introduction

Gas hydrates are crystalline structures in which water forms cavities that enclathrates small non-polar molecules, so-called guest molecules, like for instance $CO_2$ or $CH_4$. Macroscopically the structure looks similar to ice or snow but unlike ice these hydrates are also stable at temperatures above 0 °C. The enclathrated molecules stabilize the hydrate through their volume and interactions with the water molecules which constitutes the cavity walls. Hydrate can form and grow from an aqueous solution of guest molecules if pressure, temperature and concentrations of these molecules are favourable. Historically the importance of hydrates has been dominated by the industrial problems related to hydrocarbon hydrate formation in equipment and pipelines during processing and transport. Initial formation of hydrate on the interface between methane and water will eventually result in a closing film of methane hydrate characterized by a very low rate of transport of methane and water across the hydrate film. At this stage the hydrate growth will be dominated by support of methane from the solution. During more recent years the interest in hydrates has expanded in other directions. The total amount of energy related to hydrocarbons trapped in hydrate may be more than twice the amount of all known resources of coal and natural hydrocarbon sources. A thorough understanding of the kinetics of hydrate is needed to exploit these resources. Storage of $CO_2$ in reservoirs is today one of the most promising approaches for safe long terms storage of $CO_2$ as a means of reducing the emissions to the atmosphere. Relative to the storage in reservoirs with low-temperature zones, formation of hydrate may considerably reduce the rate of leakage from the reservoir. The kinetics and mechanisms of hydrate formation as well as hydrate dissociation is essential in order to understand the potential leakage rates through the hydrate. Knowledge on the rate-limiting mechanisms for the kinetics will make it possible to establish simplified correlations that can be implemented in reservoir modelling tools.

## 2. Phase-field theory

A phase-field theory has previously been applied to describe the formation of $CO_2$ hydrate in aqueous

*Corresponding author. Fax: +47 55 58 94 40.
*E-mail address:* atle.svandal@ift.uib.no (A. Svandal).

0022-0248/$ - see front matter © 2005 Elsevier B.V. All rights reserved.
doi:10.1016/j.jcrysgro.2005.11.071

solutions [1]. Here a similar version is applied to model the growth of $CO_2$ and $CH_4$ hydrate. The solidification of hydrate is described in terms of the scalar phase field $\phi$ and the local solute concentration $c$. The field $\phi$ is a structural order parameter assuming the values $\phi = 0$ in the solid and $\phi = 1$ in the liquid. Intermediate values correspond to the interface between the two phases. Only a short review of the model will be given here. Full details of the derivation and numerical methods can be found elsewhere [1–4]. The starting point is a free energy functional.

$$F = \int \mathrm{d}r^3 \left[\frac{1}{2}\varepsilon^2 T|\nabla\phi|^2 + f(\phi, c)\right]. \tag{1}$$

With $\varepsilon$ a constant, $T$ is the temperature and the integration is over the system volume. In this paper we use $c$ for concentration with units moles per volume and the mole fraction of $CO_2$ is termed $x$ and is dimensionless. Assuming equal molar volume for the two components the following relation: $c = x/v_m$ can be applied, where $v_m$ is the average molar volume. The range of the thermal fluctuations is on the order of the interfacial thickness and, accordingly, $\varepsilon$ may be fixed from knowledge of this thickness. The gradient term is a correction to the local free energy density $f(\phi, c)$. To ensure minimization of the free energy and conservation of mass, the governing equations can be written as

$$\dot{\phi} = -M_\phi \frac{\delta F}{\delta \phi}, \tag{2}$$

$$\dot{c} = \nabla\left(M_c \nabla \frac{\delta F}{\delta c}\right), \tag{3}$$

where $M_c$ and $M_\phi$ are the mobilities associated with coarse-grained equation of motion, which in turn are related to their microscopic counterparts. To reproduce bulk fluid diffusion $M_c = Dx(1-x)/RT$, where $D = D_s + (D_l - D_s)p(\phi)$ is the diffusion coefficient with $D_l = 1.0 \times 10^{-9}\,\mathrm{m^2/s}$ the diffusion coefficient in the liquid [5] and $D_s = 1.1 \times 10^{-12}\,\mathrm{m^2/s}$ for the solid [6] at 1 °C. For temperatures below 10 °C the diffusion coefficient in water for methane and carbon dioxide are the same. The hydrate diffusion is assumed to be the same for the two guest molecules in the hydrate as well. The local free energy density is assumed to have the form

$$f(\phi, c) = wT g(\phi) + [1 - p(\phi)]f_S(c) + p(\phi)f_L(c), \tag{4}$$

where the "double well" and "interpolation" functions have the forms $g(\phi) = 1/4\phi^2(1-\phi)^2$ and $p(\phi) = \phi^3(10 - 15\phi + 6\phi^2)$, which emerge from the thermodynamically consistent formulation of the theory [4]. The parameter $w$ is proportional to the interfacial free energy and can be deduced from experimental measurements [7] or predicted from molecular simulations of representative model systems [8]. Work along these lines is in progress [9] for the liquid water/hydrate interface. For this work the applied value used was the experimental value for water/ice reported [7] as $29.1\,\mathrm{mJ/m^2}$ [7].

### 2.1. Fluid thermodynamics

The free energy density is calculated as

$$v_m f_L = x\mu_c + (1-x)\mu_w. \tag{5}$$

Here $\mu_c$ and $\mu_w$ are the chemical potentials of the guest molecule and water, respectively. In general we have

$$\mu_c = \mu_c^\infty(T) + RT\ln(x\gamma_c). \tag{6}$$

Here $\mu_c^\infty(T)$ is the chemical potential at infinite dilution of component $c$ in water. $R$ is the universal gas constant and $\gamma_c$ is the activity coefficient of the guest in an aqueous solution in the asymmetric convention ($\gamma_{CO_2}$ is unity in the limit as $x$ goes to zero). For water we have

$$\mu_w = \mu_w^{\mathrm{pure}}(T) + RT\ln((1-x)\gamma_w). \tag{7}$$

Here $\mu_w^{\mathrm{pure}}(T)$ is the chemical potential of pure water. The activity coefficient of water can be obtained through the Gibbs–Duhem relation.

$$x\,d\ln(\gamma_c) + (1-x)\,d\ln(\gamma_w). \tag{8}$$

The thermodynamic properties can be estimated by considering the equilibrium between liquid and aqueous $CO_2/CH_4$, $\mu_c^L = \mu_c^{aq}$. Where the aqueous part is given by Eq. (6) and the fluid thermodynamics can be calculated by a proper equation of state. For the $CO_2$ system we have used the equation of state by Span and Wagner [10], and saturation data have been obtained from the model by Diamond and Akinfiev [11]. The chemical potential at infinite dilution is found from molecular dynamics simulations, and for 274.15 K it is $\mu_{CO_2}^\infty = -19.67\,\mathrm{kJ/mol}$. This has been taken as a reference level for the absolute thermodynamics, and Eq. (8) has then been applied to obtain the temperature dependence of $\mu_{CO_2}^\infty$.

$$\mu_{CO_2}^\infty(T) = \sum_{i=0}^{2} \frac{k_i}{T^i}. \tag{9}$$

The activity coefficient has then been fitted to a polynomial expansion in $x$.

$$\ln(\gamma_{CO_2}) = \sum_{i=1}^{2} k_i x^i. \tag{10}$$

For the methane a SRK-equation of state has been used [12], and saturation data have been extracted from the experimental article of Lekvam and Bishnoi [13]. The solubility of methane in water is much less than that of carbon dioxide, for methane the activity coefficient was assumed to be approximately equal to unity and thus ignored in the calculations. The solubility data have been used to obtain an expression of the chemical potential at infinite dilution.

$$\mu_{CH_4}^\infty(T) = \sum_{i=1}^{3} \frac{k_i}{T^i}. \tag{11}$$

All coefficients in Eqs. (9–11) are listed in Table 1.

Table 1
Coefficients in Eqs. (9–11)

| | $\mu^{\infty}_{CO_2}$ | $\mu^{\infty}_{CH_4}$ | $\ln(\gamma_{CO_2})$ |
|---|---|---|---|
| $k_0$ | $2.94351 \times 10^4$ | $-6.67663 \times 10^4$ | 0.0 |
| $k_1$ | $-1.58764 \times 10^7$ | $3.42857 \times 10^7$ | $-1.74497$ |
| $k_2$ | $6.61845 \times 10^8$ | $-5.14493 \times 10^9$ | $1.06389 \times 10^2$ |

### 2.2. Hydrate thermodynamics

The thermodynamics of the hydrate is based on the model by Kvamme and Tanaka [14] and van der Waals and Platteeuw [15]. The free energy in the liquid was calculated as

$$v_m f_S = x\mu^H_{CO_2} + (1-x)\mu^H_w. \quad (12)$$

The expression for the chemical potential for water in hydrate with one type of guest molecule is

$$\mu^H_w = \mu^{0,H}_w + \sum_j RTv_j \ln(1-\theta_j). \quad (13)$$

Here $\mu^{0,H}_w$ is the chemical potential for water in an empty hydrate structure. The sum is over small and large cavities, where $v_j$ is the number of type $j$ cavities per water molecule. $\theta_j$ is the filling fraction of cavity $j$ given as $\theta_j = x_j/(v_L(1-x_j))$, where $x_j$ is the molar fraction with respect to cavity $j$ only. The chemical potential for the guest molecule is

$$\mu^H_c = \Delta g^{inc}_{c,j} + RT \ln\left(\frac{\theta_j}{1-\theta_j}\right). \quad (14)$$

Here $\Delta g^{inc}_{c,j}$ is the free energy of inclusion of guest molecule $c$ in cavity $j$. Assuming that the chemical potential in the different cavity types are equal, an expression for the ratio between the filling fractions was obtained. Requiring that the specific mole fractions add up to the total mole fraction ($x_{small} + x_{large} = x$), and solving a second-order equation, an expression for the chemical potentials as a function of the total mole fraction $x$ was obtained. The total free energies as a function of mole fraction, with temperature 1 °C and pressure 150 bar, are shown in Fig. 1. The main difference between $CH_4$ and $CO_2$ hydrate is that while $CO_2$ only occupies the large cavities, methane goes into both large and small cavities. This allows for a higher guest molecule concentration in the methane hydrate.

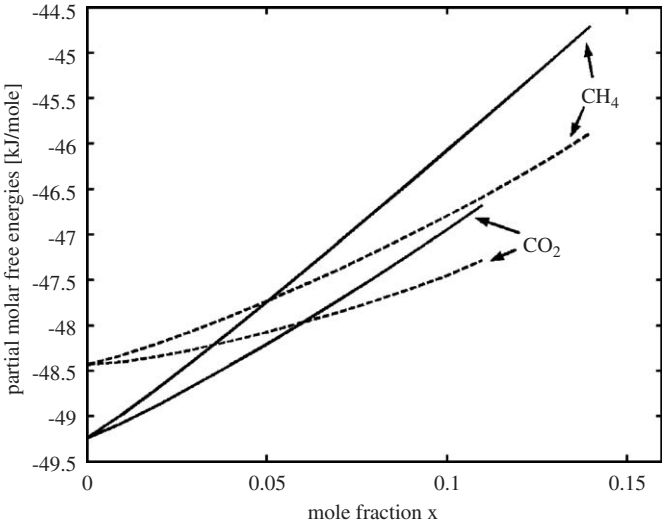


Fig. 1. Free energies of methane and carbon dioxide hydrate (dashed lines) and the aqueous solutions (solid lines) as a function of the mole fraction.

## 3. Hydrate growth simulations

### 3.1. Numerical results

The model has been implemented with both planar and circular geometries for methane and carbon dioxide hydrate. The temperature is normally chosen to be 1 °C to obtain a high driving force without going into the region of ice. Most of the simulations have been done at 150 bar to assure a high driving force. No flux boundary conditions at the walls were assumed and the grid resolution used was 0.4 nm. The time step was $1.6 \times 10^{-12}$ s. Initially a supersaturated water solution and a hydrate nucleus/film with radius/thickness 4 nm were assumed. The supersaturated solution is representing the meta-stable equilibrium between water and liquid $CO_2/CH_4$. The movement of the front was tracked by following the $\phi = 0.5$ value. In Fig. 2 simulations of methane hydrate growth is shown at 3 different pressures. For high driving forces (as for $CO_2$ hydrate and for $CH_4$ hydrate with circular geometry and high pressure) the simulations follows perfectly a power law $\propto t^{1/2}$, indicating a diffusion-controlled process. Under conditions with lower driving forces the simulations show some deviation from this initially, but the long time behaviour diverges towards the same power law. Fig. 3 shows the interface velocities for methane and carbon dioxide hydrate with circular and planar geometries at 1 °C and 150 bar. Since the simulations yield the growth process to be controlled by the diffusion, three very important parameters in the simulations are the composition in the growing hydrate, the initial mole fraction of the guest molecule in water and the equilibrium mole fraction of the guest molecule between the two phases. Solving simultaneously the equilibrium equations in the two phases with respect to the chemical potential of the components, the equilibrium conditions at different pressures and temperatures was obtained. It was found that as the pressure was increased more gas molecules were available in the solution, and less molecules were needed to keep the hydrate stable. The fact that the growth rate increases with pressure is better accounted for by this effect than by changes in the chemical driving force itself.

### 3.2. Anisotropy

In contrast to isotropic growth where the two model parameters $\varepsilon$ and $w$ are fixed through information on the

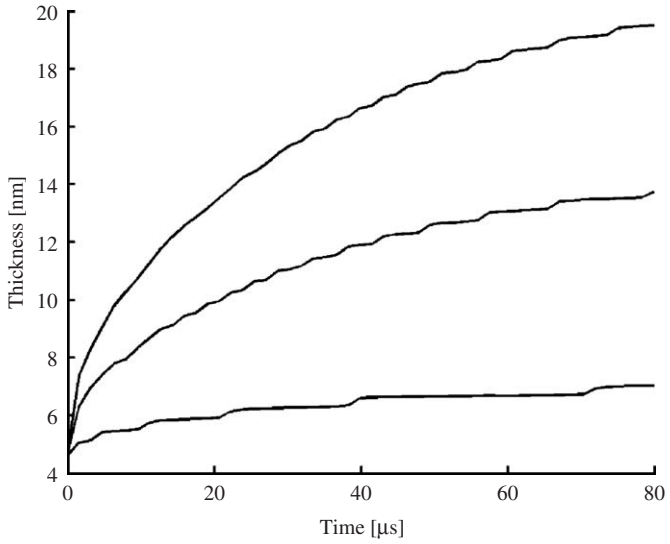


Fig. 2. Thickness of the hydrate film as a function of time. Upper line is 150 bar, middle line is 100 bar and the lower line is 50 bar.

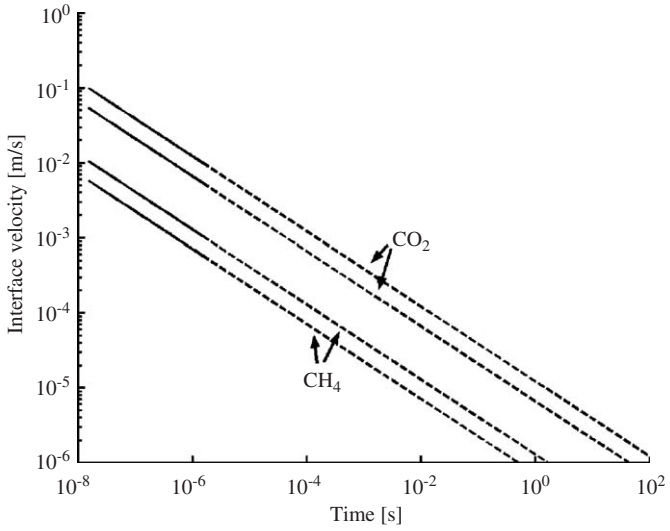


Fig. 3. Velocity of the interface as a function of time. The solid lines show the actual simulations, while the dashed lines are extrapolations into experimental time-scales. From the top down the lines are: circular $CO_2$, planar $CO_2$, circular $CH_4$ and planar $CH_4$.

interfacial properties there is no similar theoretical relationship to relate anisotropic crystal growth. On the other hand, at the cost of a few empiric model parameters the phase field approach has proven [2,3] to be able to reproduce the growth of many experimentally observed crystal structures. The relative impact of these orientational effects on kinetic growth rates and kinetic limiting contributions is an important issue. For this purpose Eq. (1) is extended with an orientation field [2], and the constant $\varepsilon$ is assumed to be directional dependent, expressed as

$$\varepsilon = \varepsilon'\left[1 + \frac{s_0}{2}\cos(n\vartheta - 2\pi\theta)\right]. \quad (15)$$

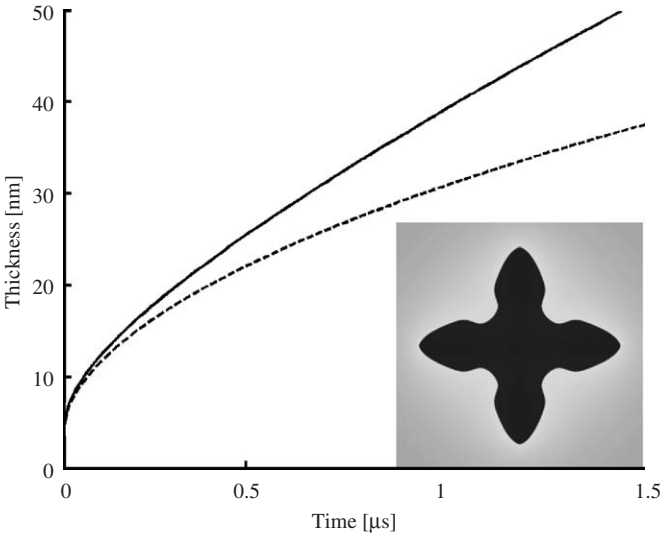


Fig. 4. Anisotropic growth (solid line) compared to isotropic growth (dashed line). The picture shows the dendrite at the end of the simulated time.

Here $s_0$ is the anisotropic amplitude, $n$ is the symmetry, $\theta$ is the introduced orientation field and $\vartheta = \arctan[(\nabla\phi)_y/(\nabla\phi)_x]$. The interface velocity for the dendritic growth should theoretically approach a constant value. The results from our anisotropic simulations yield a faster growth rate than the isotropic approaching a linear behaviour as expected. The simulations are unfortunately computationally expensive and the results shown in Fig. 4 have not diverged towards a steady growth rate yet.

## 4. Conclusions

Phase-field theory simulations have been applied to model the growth of $CH_4$ and $CO_2$ hydrates from respective aqueous solutions of these hydrate formers. Presently there are no experimental data available for direct comparisons to the predictions presented here and the main purpose of this paper has been to demonstrate the approach and the corresponding parameterization. As expected relative to the differences in solubility of the two components in water the kinetic rates of $CO_2$ hydrate growth is larger than that of $CH_4$ hydrate. The rate of circular growth is larger than the corresponding growth on a planar interface but in both cases the kinetics is dominated by the mass transport of solutes towards the growing front. We have also investigated the effects of anisotropy. The growth of dendrites is faster than for isotropic growth and are approaching a constant rate.

## Acknowledgments

Financial support from the Norwegian Research Council through project 101204, and from Conoco-Phillips, is highly appreciated.

## References

[1] B. Kvamme, A. Graue, E. Aspenes, T. Kuznetsova, L. Grànàsy, G. Tòth, et al., Phys. Chem. Chem. Phys. 6 (2004) 2327.
[2] L. Grànàsy, T. Börzsönyi, T. Pusztai, Phys. Rev. Lett. 88 (2002) 206105.
[3] J.A. Warren, W.J. Boettinger, Acta Metall. Mater. 43 (1995) 689.
[4] S.L. Wang, R.F. Sekerka, A.A. Wheeler, B.T. Murray, S.R. Coriell, R.J. Braun, et al., Physica D 69 (1993) 189.
[5] G. Rehder, S.H. Kirby, W.B. Durham, L.A. Stern, E.T. Peltzer, J. Pinkston, et al., Geochem. Cosmochim. Acta 68 (2004) 285.
[6] R. Radhakrishnan, A. Demurov, H. Herzog, B.L. Trout, Energ. Convers. Manage. 44 (2003) 771.
[7] S.C. Hardy, Philos. Mag. 35 (1977) 471.
[8] R.L. Davidchack, B.B. Laird, J. Chem. Phys. 108 (1998) 9452.
[9] T. Kuznetsova, B. Kvamme, work in progress, 2005.
[10] R. Span, W. Wagner, J. Phys. Chem. Ref. Data 25 (1996) 1509.
[11] L.W. Diamond, N.N. Akinfiev, Fluid Phase Equilibria 208 (2003) 265.
[12] G. Soave, Chem. Eng. Sci. 27 (1972) 1197.
[13] K. Lekvam, P.R. Bishnoi, Fluid Phase Equilibria 131 (1997) 297.
[14] B. Kvamme, H. Tanaka, J. Phys. Chem. 99 (1995) 7114.
[15] J.H.v.d. Waals, J.C. Platteeuw, Adv. Chem. Phys. 2 (1959) 1.